Separation Science and Technology
Publication details, including instructions for authors and subscription information:
http://www.informaworld.com/smpp/title~content=t713708471

Intraparticle Diffusion/Convection Models for Pressurization and Blowdown of Adsorption Beds with Langmuir Isotherm

Z. P. Lu[a]; J. M. Loureiro[a]; M. D. LeVan[b]; A. E. Rodrigues[c]
[a] LABORATORY OF SEPARATION AND REACTION ENGINEERING, SCHOOL OF ENGINEERING UNIVERSITY OF PORTO, PORTO CODEX, PORTUGAL [b] DEPARTMENT OF CHEMICAL ENGINEERING, UNIVERSITY OF VIRGINIA, CHARLOTTESVILLE, VIRGINIA, USA [c] LABORATORY OF SEPARATION AND REACTION ENGINEERING, SCHOOL OF ENGINEERING, UNIVERSITY OF PORTO, PORTO CODEX, PORTUGAL

To cite this Article Lu, Z. P. , Loureiro, J. M. , LeVan, M. D. and Rodrigues, A. E.(1992) 'Intraparticle Diffusion/Convection Models for Pressurization and Blowdown of Adsorption Beds with Langmuir Isotherm', Separation Science and Technology, 27: 14, 1857 — 1874
To link to this Article: DOI: 10.1080/01496399208019454
URL: http://dx.doi.org/10.1080/01496399208019454

SEPARATION SCIENCE AND TECHNOLOGY, 27(14), pp. 1857–1874, 1992

Intraparticle Diffusion/Convection Models for Pressurization and Blowdown of Adsorption Beds with Langmuir Isotherm

Z. P. LU and J. M. LOUREIRO
LABORATORY OF SEPARATION AND REACTION ENGINEERING
SCHOOL OF ENGINEERING
UNIVERSITY OF PORTO
4099 PORTO CODEX, PORTUGAL

M. D. LEVAN
DEPARTMENT OF CHEMICAL ENGINEERING
UNIVERSITY OF VIRGINIA
CHARLOTTESVILLE, VIRGINIA 22903-2442, USA

A. E. RODRIGUES*
LABORATORY OF SEPARATION AND REACTION ENGINEERING
SCHOOL OF ENGINEERING
UNIVERSITY OF PORTO
4099 PORTO CODEX, PORTUGAL

Abstract

Intraparticle diffusion/convection and equilibrium models are used to simulate the bed dynamics of pressurization and blowdown steps of PSA processes with binary mixtures of inert and adsorbable species. The effect of the nature of the equilibrium isotherm, i.e., linear and Langmuir isotherms, is discussed. The improvement of mass transfer inside the adsorbent by increasing particle permeability or decreasing particle size is addressed. Simulation results show that using "large-pore" adsorbents, i.e., increasing permeability to cause a high intraparticle convective flow instead of decreasing particle size to reduce intraparticle mass transfer resistances, is a good choice in PSA processes.

INTRODUCTION

Pressure gradients in the bed during pressurization and blowdown steps of PSA processes are receiving more and more attention. The analysis of

*To whom correspondence should be addressed.

pressurization and blowdown was carried out by Sundaram and Wankat (*10*); however, their model is only valid for inert or trace adsorbable gases. The importance of axial pressure gradients during pressurization and blowdown was experimentally studied by Hart et al. (*1*) using inert mixtures or adsorbable species alone. The mass transfer resistance inside adsorbents (micropore + macropore) was first considered in a nonisothermal model (*11*) to simulate the bed behavior of pressurization and blowdown, but the cases studied were still limited to species of the same kind (inert or adsorbable). Rodrigues et al. (*8*) used an equilibrium model with a binary mixture (inert + adsorbable species) to assess the bed dynamics during pressurization. Several situations depending on the pressure ratio, feed, and initial concentrations were discussed, and the prediction of the penetration distance for an initially clean bed was first derived. The Darcy equation was used as the momentum balance equation in all the works mentioned above.

The difference in the bed dynamic behavior when using Darcy or Ergun momentum equations was discussed, and general equations for the penetration distance were shown by Rodrigues et al. (*9*) and Lu et al. (*3*); also, the mole fraction plateaus at the bed outlet during blowdown were predicted and compared with numerical simulation results.

An interesting topic in the areas of separation and reaction engineering is the "augmented" effective diffusivity by the intraparticle forced convective flow in "large-pore" materials (*5–7*). The improvement of the bed performance by intraparticle convective flow during pressurization and blowdown was assessed by Lu et al. (*4*).

The objective of this paper is to assess the effect of the permeability of the adsorbent and of its size in diffusion/convection models (*2*) with a Langmuir equilibrium isotherm.

MATHEMATICAL MODELS

The system considered here is an isothermal bed packed with "large-pore" adsorbent material (slab geometry); during pressurization, the feed is a binary mixture of Species A (adsorbable) and B (inert). The adsorption equilibrium isotherm is given by the relation

$$q_A = \frac{k_1 c_A}{(1 + k_2 c_A)} = \frac{q^* k c_A}{1 + (k - 1)c_A/c_h}$$

Initially the bed is clean at a pressure $P = P_l$ for pressurization and has a nonuniform concentration at $P = P_h$ for blowdown. At time $t = 0$, a positive (for pressurization) or a negative (for blowdown) step change on

total pressure is made at the bed inlet. Model equations in dimensionless form, for the intraparticle diffusion/convection model, are given below using the following variables:

$$x = \frac{z}{L}, \qquad \rho = \frac{z'}{l}, \qquad f = \frac{c}{c_0} = \frac{P}{P_0},$$

$$f' = \frac{c'}{c_0} = \frac{P'}{P_0}, \qquad u^* = \frac{u}{u_0}, \qquad v^* = \frac{v}{v_0}, \qquad \theta = \frac{t}{\tau_0}$$

where c_0 is the total concentration at atmospheric pressure, v_0 is a reference intraparticle velocity, τ_0 is the reference space time, and u_0 is the bulk fluid superficial velocity at the bed inlet in steady-state at a given pressure drop $\Delta P_0 = P_h - P_l$ (here $P_l = P_0$).

Mass balance inside the adsorbent particle:

$$\frac{\partial}{\partial \rho}\left(\frac{f'}{b_4 + f'}\frac{\partial y'_A}{\partial \rho} + \frac{y'_A}{b_4}\frac{\partial f'}{\partial \rho}\right) - \lambda_0 \frac{\partial (v^* f' y'_A)}{\partial \rho}$$

$$= \alpha_0 \left[1 + \frac{1 - \epsilon_p}{\epsilon_p}\frac{kq^*}{(1 + (k-1)\Phi f' y'_A)^2}\right]\frac{\partial (f' y'_A)}{\partial \theta} \quad (1)$$

$$\frac{\partial}{\partial \rho}\left(\frac{1}{b_4}\frac{\partial f'}{\partial \rho}\right) - \lambda_0 \frac{\partial (v^* f')}{\partial \rho}$$

$$= \alpha_0 \left[\frac{\partial f'}{\partial \theta} + \frac{1 - \epsilon_p}{\epsilon_p}\frac{kq^*}{(1 + (k-1)\Phi f' y'_A)^2}\frac{\partial (f' y'_A)}{\partial \theta}\right] \quad (2)$$

with boundary conditions:

$$\rho = 0, \; y'_A = y_A - \frac{\partial y_A}{\partial x}\beta_R; \qquad f' = f - \frac{\partial f}{\partial x}\beta_R \quad (3)$$

$$\rho = 1, \; y'_A = y_A + \frac{\partial y_A}{\partial x}\beta_R; \qquad f' = f + \frac{\partial f}{\partial x}\beta_R \quad (4)$$

and initial condition:

$$\theta = 0, \; y'_A = y_A; \qquad f' = f; \qquad \forall x, \rho \quad (5)$$

Momentum equation for the fluid inside particle:

$$v^* = \frac{v}{v_0} = -\beta_l \frac{\partial f'}{\partial \rho} \tag{6}$$

Mass balances for the bulk fluid phase in a bed volume element: Species A:

$$\frac{\partial}{\partial x}\left(\frac{u^* f}{\mathrm{Pe}} \frac{\partial y_A}{\partial x}\right) - \frac{\partial (u^* f y_A)}{\partial x} = \frac{\partial (f y_A)}{\partial \theta} + \frac{1-\epsilon}{\epsilon} N_A \tag{7}$$

Overall:

$$\frac{\partial (u^* f)}{\partial x} + \frac{\partial f}{\partial \theta} + \frac{1-\epsilon}{\epsilon} N = 0 \tag{8}$$

where dimensionless fluxes of Species A and overall are given by

$$N_A = \frac{\epsilon_p}{\alpha_0}\left[\left(-\frac{f'}{b_4 + f'} \frac{\partial y'_A}{\partial \rho} - \frac{y'_A}{b_4} \frac{\partial f'}{\partial \rho} + \lambda_0 v^* f' y'_A\right)\Big|_{\rho=0} - \left(-\frac{f'}{b_4 + f'} \frac{\partial y'_A}{\partial \rho} - \frac{y'_A}{b_4} \frac{\partial f'}{\partial \rho}\right) + \lambda_0 v^* f' y'_A\Big)\Big|_{\rho=1}\right] \tag{9}$$

$$N = \frac{\epsilon_p}{\alpha_0}\left[\left(-\frac{1}{b_4} \frac{\partial f'}{\partial \rho} + \lambda_0 v^* f'\right)\Big|_{\rho=0} - \left(-\frac{1}{b_4} \frac{\partial f'}{\partial \rho} + \lambda_0 v^* f'\right)\Big|_{\rho=1}\right] \tag{10}$$

Momentum equation for the bulk fluid:

$$-\frac{\partial f}{\partial x} = b_5 u^* + b_6 f (u^*)^2 \tag{11}$$

Boundary conditions associated with Eqs. (9) and (10) are: Pressurization:

$$x = 0,\ y_A - \frac{1}{\mathrm{Pe}} \frac{\partial y_A}{\partial x} = y_f; \qquad f = f_h \tag{12}$$

$$x = 1,\ \frac{\partial y_A}{\partial x} = 0; \qquad \frac{\partial f}{\partial x} = 0 \tag{13}$$

Blowdown:

$$x = 0, \frac{\partial y_A}{\partial x} = 0; \qquad f = f_l \tag{14}$$

$$x = 1, \frac{\partial y_A}{\partial x} = 0; \qquad \frac{\partial f}{\partial x} = 0 \tag{15}$$

The initial condition associated with Eqs. (9) and (10) is: Pressurization:

$$\theta = 0, y_A = 0; \qquad f = f_l; \qquad \forall x > 0 \tag{16}$$

Blowdown:

$$\theta = 0, y_A = \begin{cases} 0 & x \geq 0.9 \\ y_0(0.9 - x)/0.3 & 0.6 < x < 0.9; \\ y_0 & x \leq 0.6 \end{cases} \qquad f = f_h; \qquad \forall x > 0 \tag{17}$$

The definitions of the parameters, β_R, β_l, b_4, b_5, b_6, q^*, k, Pe, λ, λ_0, α, α_0, and Φ can be found in Table 1.

We call the "complete" case above, the diffusion/convection model, Case A. If $\lambda_0 = 0$, the diffusion/convection is reduced to the diffusion model, which is called Case B. If there are no mass transfer resistances inside the adsorbent, the model above is reduced to the equilibrium model which is called Case C.

TABLE 1
The Definitions of the Parameters

$b_4 = \frac{D_{mo}}{D_k}$	$q^* = \frac{k_1}{1 + k_2 c_h}$
$b_5 = \frac{150\mu(1 - \epsilon)^2 L}{d_p^2 \epsilon^3 P_0} u_0$	$k = 1 + k_2 c_h$
$b_6 = \frac{1.75\rho_0(1 - \epsilon)L}{P_0 d_p \epsilon^3} u_0^2$	$\frac{1}{\text{Pe}} = \frac{\epsilon D_{ax}}{Lu}$
$\beta_R = \frac{l}{2L}$	$\lambda = \lambda_0 v^*(b_4 + f')$
$\beta_l = \frac{L}{l}\frac{P_0}{\Delta P_0}$	$\lambda_0 = \frac{\tau_f l^2}{D_{mo}}\frac{v_0}{\epsilon_p l}$
$\Phi = \frac{P_l}{P_h}$	$\alpha = \alpha_0 u^*(b_4 + f')$
	$\alpha_0 = \frac{\tau_f l^2}{D_{mo}}\frac{u_0}{\epsilon L}$

SIMULATION RESULTS AND DISCUSSION

The commercial PDECOL package was used to solve the sets of Eqs. (1)–(17). Details can be found elsewhere (*2*). The calculation was stopped when $|f_h - f_{(x=1)}|/f_h < 1\%$ for pressurization and $|f_l - f_{(x=1)}|/f_l < 1\%$ for blowdown. This enables us to calculate pressurization and blowdown times as the times needed to fulfill those conditions.

The simulation of the pressurization step used an input of a high pressure binary mixture (inert and adsorbable species) with $y_f = 0.5$ to feed the clean bed ($y_0 = 0$). The blowdown was started with an initial mole fraction profile in the bed as stated by Eq. (17) where $y_0 = 0.5$. The effects of the adsorbent size $d_p = 0.045$, 0.07, and 0.1 cm; permeability $B_p = 1.25 \times 10^{-9}$ and 5×10^{-9} cm^2; and the nature of the equilibrium isotherm $k = 1$ (linear) and 2 (Langmuir) are addressed. The base values are adsorbent capacity $q^* = Q^*\Phi = Q^*/f_h = 20$ and pressure ratio $\Phi = P_l/P_h = 0.2$, $u_0 = 135$ cm/s, and $\tau_0 = 0.446$ s. Fluid, particle, and system properties are listed in Table 2. In all figures throughout the paper, the solutions of the diffusion/convection (Case A), diffusion (Case B), and equilibrium (Case C) models are represented by solid, dotted, and dashed lines, respectively.

Nature of the Adsorption Equilibrium Isotherm

It is well known that adsorption is favorable and desorption is unfavorable in a fixed bed with a Langmuir isotherm in systems where the superficial velocity is constant. The effect of the nature of the equilibrium isotherm ($k = 1$ corresponds to a linear isotherm and $k = 2$ corresponds to a Langmuir isotherm) on the bed dynamics in pressurization and blowdown using the diffusion/convection models is similar to the one observed when the equilibrium model was used (*3*).

TABLE 2
Values of Fluid, Particle, and System Properties Used in Numerical Simulations

$D_{mo} = 0.1$ cm^2·s^{-1}	$\epsilon = 0.4$
$\rho_0 = 10^{-3}$ g·cm^{-3}	$\epsilon_p = 0.7$
$\mu = 10^{-4}$ g·cm^{-1}·s^{-1}	$L = 150$ cm
$k = 1$ and 2	$d_p = 0.1$, 0.07, and 0.045 cm
$q^* = 20$	$\tau_f = 4.5$
$P_l = P_0 = 100$ kPa	
$P_h = 500$ kPa	

Pressurization

Figures 1(a)–1(b) show the effect of k (nature of the isotherm) on the histories of mole fraction at $x = 0.1$ during pressurization of an initially clean bed, as calculated by the three models. The mole fraction wave in the bed moves at a slower velocity with a Langmuir isotherm ($k = 2$) in Case C since the adsorbed phase concentration is higher than with a linear isotherm ($k = 1$) for a given $y_f P < P_h$. Due to intraparticle mass transfer resistance in Cases A and B, the mole fraction waves move very fast at short times no matter what the nature of the isotherm is; then, at larger times, its effect is similar to that in Case C. The mole fraction histories with the diffusion model are smooth. The solution of the "complete" model shows an interesting feature: at lower times the histories are similar to the ones observed when diffusion alone is present because the intraparticle mass transfer is dominated by diffusion due to the very high intraparticle gradients of mole fraction; then, at larger times, the importance of the intraparticle convective flow increases relative to diffusion, and the histories show the improvement of the mass transport between fluid and

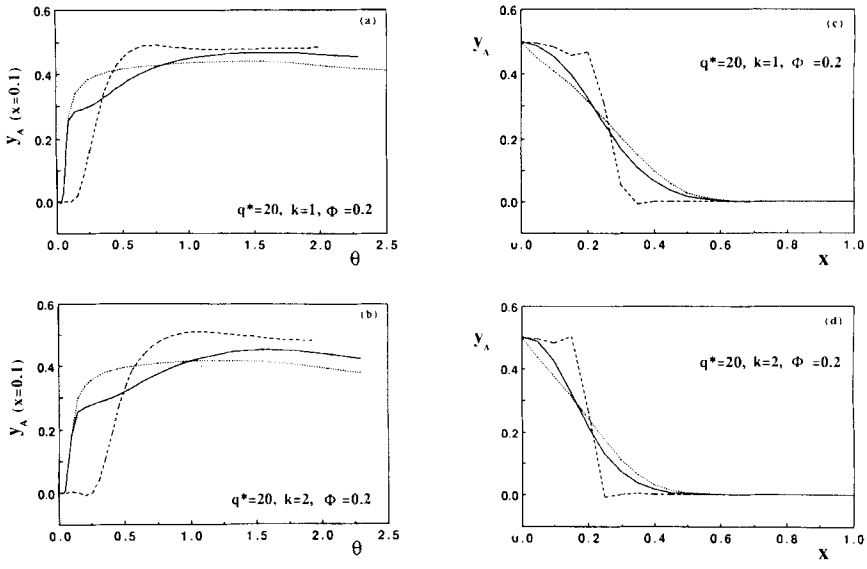

FIG. 1. Effect of the nature of equilibrium isotherm k ($d_p = 0.1$ cm, —— Case A ($B_p = 2 \times 10^{-10}$ cm^2), ··· Case B, ---- Case C) in pressurization. (a) Histories of adsorbable species mole fraction y_A at $x = 0.1$ ($k = 1$). (b) Histories of adsorbable species mole fraction y_A at $x = 0.1$ ($k = 2$). (c) Final axial profiles of adsorbable species y_A ($k = 1$). (d) Final axial profiles of adsorbable species y_A ($k = 2$).

particles through the increase of the local adsorbed quantity (approaching the adsorption equilibrium) and the corresponding lower fluid mole fraction.

The axial mole fraction profiles for a linear ($k = 1$) and a Langmuir ($k = 2$) isotherm at the end of pressurization are shown in Figs. 1(c)–1(d), as predicted by the three models. Due to the higher adsorbed phase concentration with the Langmuir isotherm (for a partial pressure lower than P_h), the penetration distance is smaller with $k = 2$. Nevertheless, the profile shapes are similar for both isotherm types. It is seen that the presence of intraparticle resistances in Case B corresponds to a more dispersive profile in this case; the profile of the "complete" Case A falls between the two limiting situations of equilibrium and diffusion alone, showing the enhancement of the system behavior (relative to diffusion alone) introduced by intraparticle convection.

The profiles of reduced pressure, mole fraction and intraparticle Peclet number at different times during pressurization are shown in Figs. 2(a)–(c), respectively, for a particle located at the axial position $x = 0.1$ in the bed. The behavior is very similar to that observed when the pressurization of an initially unclean bed is simulated (*4*). Due to the presence of intraparticle convection, in Case A the local reduced pressure keeps a plane profile at all times; on the contrary, in Case B the profiles are concave and symmetrical around the center of the particle, which does not reach the final pressure, even at the end of pressurization, i.e., $|f_h - f_{(x=1)}|/f_h < 1\%$.

At short times, transport by intraparticle diffusion dominates due to the high mole fraction gradients inside the particles, and the mole fraction profiles are similar for Cases A and B; as time increases, the convective flow (enhancing mass transfer) modifies the profiles in Case A. The final partial pressures inside the particles obtained with intraparticle convection are higher than with diffusion alone, clearly showing the enhancement of mass transport between fluid and solid, i.e., with intraparticle convection (Case A) the adsorbent is almost saturated at the local partial pressure in the bed at the end of pressurization, while without convection (Case B) the adsorbent stays far from saturation. Moreover, intraparticle mole fraction profiles can be asymmetric for intraparticle diffusion/convection models as shown in Fig. 2(b).

The profiles of the intraparticle Peclet number λ in a particle located at the axial position $x = 0.1$ in the bed, shown in Fig. 2(c), are somehow different from the profiles at $x = 0$ (*4*). This happens because the pressure wave arrives immediately at $x = 0$, while it takes some time to arrive at $x = 0.1$. It is seen that λ increases and then decreases at $x = 0.1$, the flat profile being established only at the end of pressurization.

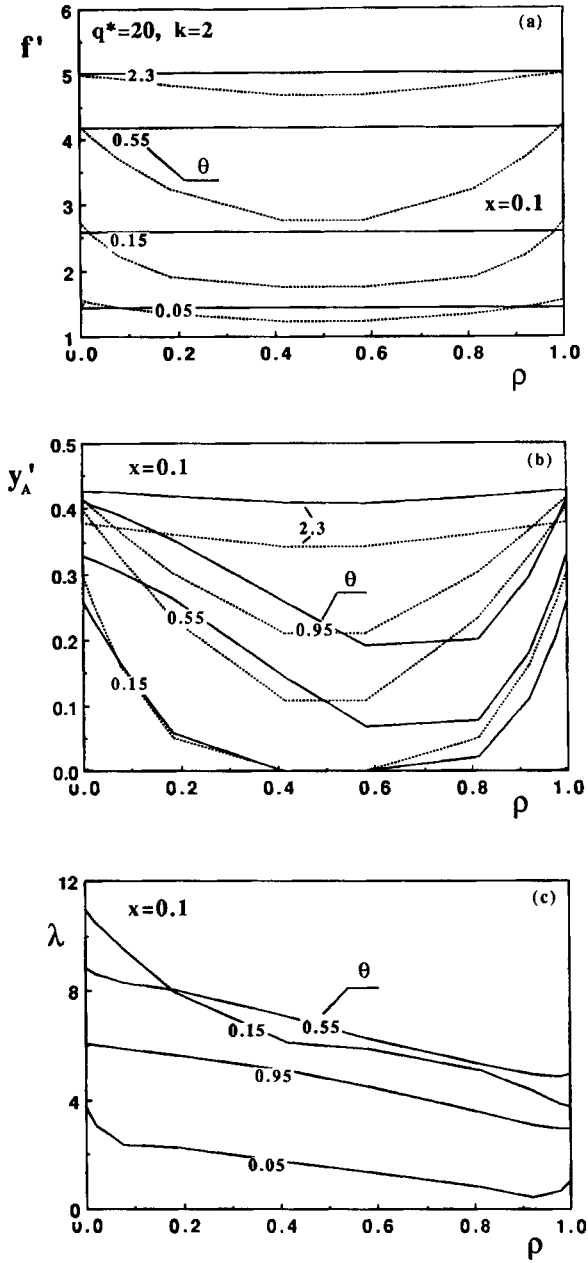

FIG. 2. Intraparticle profiles of (a) reduced total pressure f', (b) mole fraction y'_A, and (c) intraparticle Peclet number λ, at $x = 0.1$ during pressurization ($k = 2$, $d_p = 0.1$ cm, —— Case A ($B_p = 2 \times 10^{-10}$ cm^2), ··· Case B.

Blowdown

The histories of mole fraction y_A and mole flux $(-u^*y_A)$ at the column outlet ($x = 0$) during blowdown of a bed with a nonuniform initial mole fraction profile for both isotherm types and the three models are shown in Figs. 3(a)–(b). The effect of the nature of the isotherm is clearer with this initial condition than with an initial uniform concentration (*3*, *4*).

The first mole fraction plateau at the outlet, observed with the equilibrium model, is smoothed out by intraparticle resistances (diffusion model) and is recovered when intraparticle convection develops; the value of this plateau is unchanged relative to the blowdown of a bed with an initial uniform concentration (*3*). However, the second mole fraction plateau is lower with this new initial condition, since the initial quantity inside the bed is lower. Moreover, the enhancement of mass transfer due to convection is now more clear, since the second plateau is model-dependent in this situation, contrary to the uniform initial concentration studied before (*4*). The final quantity remaining in the bed is lower with the equilibrium model and higher with the diffusion model, the complete case falling in between. The same is seen in Figs. 3(c)–3(d), where the mole flux at the outlet at short times decreases when going from equilibrium to diffusion-

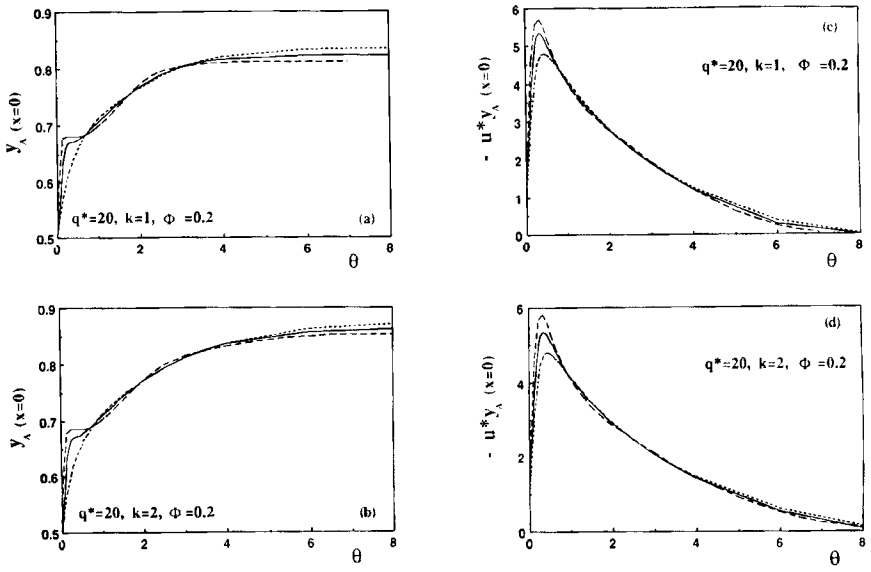

FIG. 3. Histories of (a and b) mole fraction y_A and (c and d) mole flux $(-u^*y_A)$ at the open end ($x = 0$) during blowdown for $k = 1$ and $k = 2$ ($d_p = 0.1$ cm, —— Case A ($B_p = 2 \times 10^{-10}$ cm^2), ··· Case B, ---- Case C).

controlled situations, showing the improvement of the adsorbent regeneration by intraparticle convection relative to diffusion.

The same conclusions can be drawn from the analysis of Figs. 4(a)–(c), where the profiles along the bed of reduced total pressure f, reduced velocity $(-u^*)$, and mole fraction are shown for various times during blowdown. Figure 4(b) shows that some peaks develop in the axial profiles of reduced velocity both with the diffusion and (mainly) with the diffusion/convection models. The increase of the peaks by intraparticle convection is due to the increase of the local desorption near the bed outlet (faster mass transfer between solid and fluid) with the associated increase of the local total pressure which corresponds to a lower pressure gradient and a lower velocity a little further down the column.

The mole fraction profiles (Fig. 4c) for Case A are again between the profiles for Cases B and C.

Effects of the Particle Permeability B_p and Size d_p

For a given pressure drop across the particle, the larger the particle permeability B_p, the larger will be the convective flow developed inside the particles, i.e., the larger the intraparticle Peclet number λ.

The increase of the convective flow can be measured by the "apparent" diffusivity $\tilde{D}_e$ lumping diffusion and convection in a unique transfer parameter; the relation between $\tilde{D}_e$ and the true effective diffusivity D_e was given by Rodrigues et al. (*6*) to be

$$\frac{D_e}{\tilde{D}_e} = \frac{\tilde{\alpha}}{\alpha} = \frac{3}{(\lambda/2)}\left(\frac{1}{\tanh(\lambda/2)} - \frac{1}{(\lambda/2)}\right) \tag{18}$$

This equation shows that when λ increases, $\tilde{\alpha} = \tilde{\tau}_d/\tau$ decreases and $\tilde{D}_e$ increases, increasing the mass transfer (for the same system, i.e., for constant D_e). On the other hand, in the absence of intraparticle convection ($\lambda = 0$), if the particle diameter d_p is reduced, $\alpha = \tau_d/\tau$ decreases (since α is proportional to d_p^2), i.e., the intraparticle mass transfer resistance is reduced.

The increase of the performance of the bed can then be achieved by one of two strategies: increase B_p (increasing mass transfer) or decrease d_p (reducing intraparticle resistances). Their effect on the bed behavior can be equivalent as shown in Figs. 5(a)–(b) where the final axial mole fraction profiles during pressurization are represented for various permeabilities (Fig. 5a) and various particle diameters (Fig. 5b). These two figures also show that when B_p is increased (or d_p is reduced), the equilibrium situation

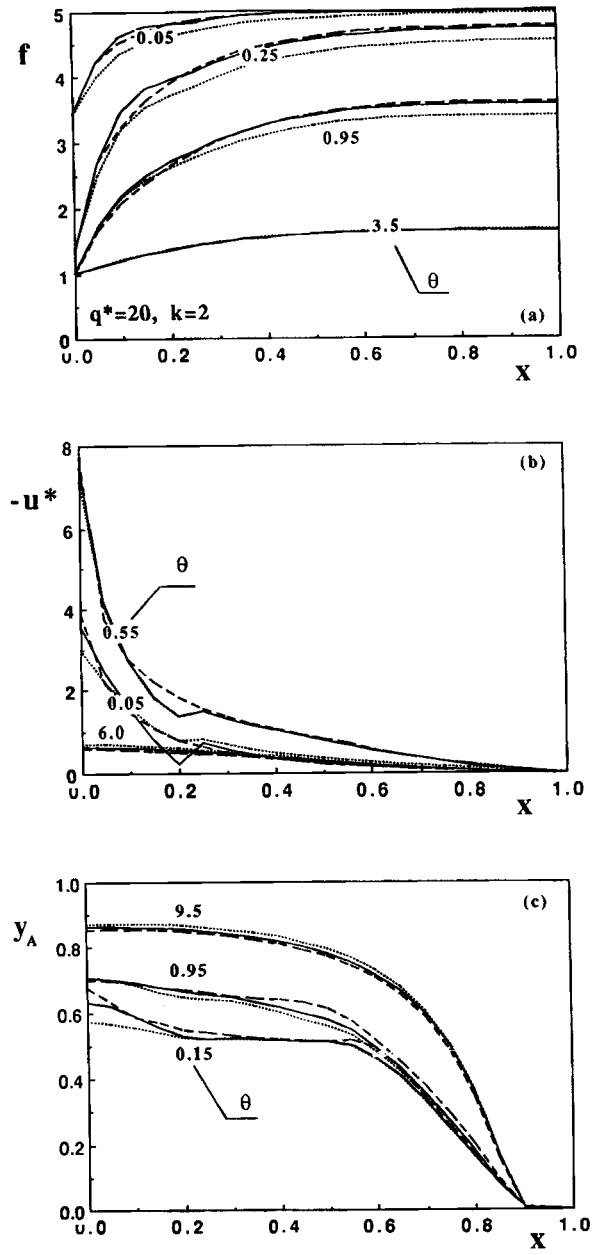

FIG. 4. Axial profiles of (a) reduced total pressure f, (b) reduced velocity $(-u^*)$ and mole fraction y_A during blowdown ($k = 2$, $d_p = 0.1$ cm, —— Case A ($B_p = 2 \times 10^{-10}$ cm^2), ··· Case B, ---- Case C).

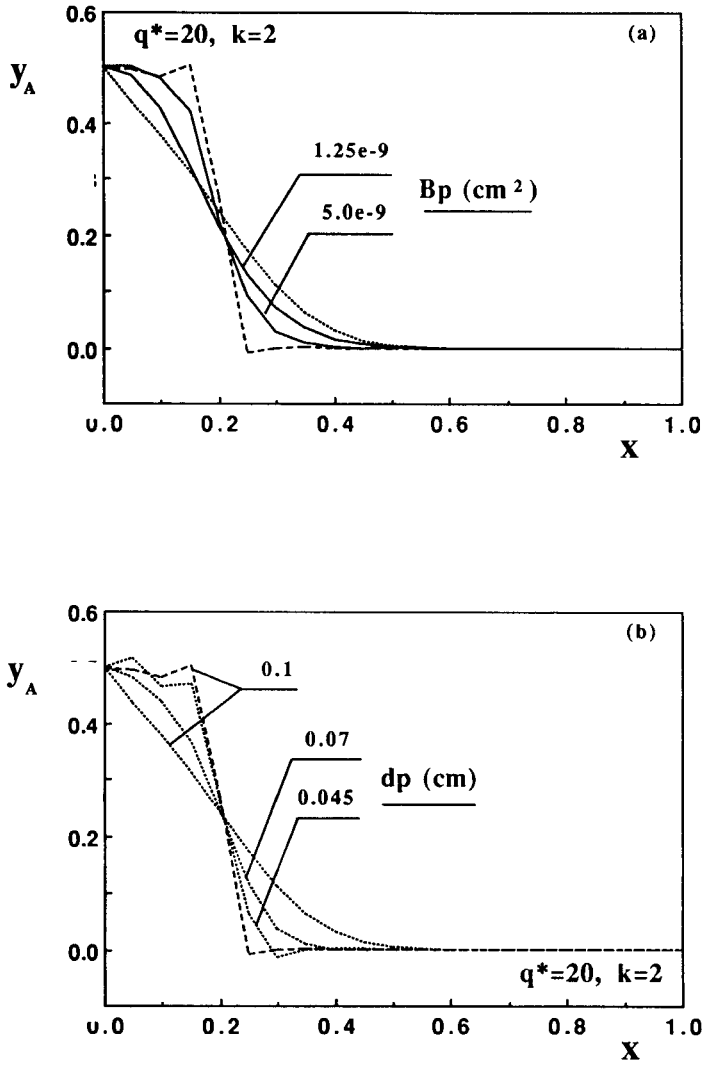

FIG. 5. Final axial mole fraction profile of adsorbable species y_A in pressurization (k = 2, —— Case A, ··· Case B, ---- Case C). (a) Effect of the particle permeability B_p (d_p = 0.1 cm, B_p = 1.25 × 10^{-9} and 5 × 10^{-9} cm^2). (b) Effect of the particle size d_p (d_p = 0.1, 0.07, and 0.045 cm).

is approached. This was shown before by Lu et al. (*2*) when dealing with the desorption of a fixed bed containing large-pore particles. However, while the increase of B_p has only a marginal effect on the other bed performance characteristics, namely pressurization and blowdown times, the same is not true when d_p is decreased.

The histories of reduced total pressure f at the closed end ($x = 1$) during pressurization and blowdown and the histories of mole fraction y_A and mole flux ($-uy_A$) at the open end ($x = 0$) during blowdown are shown in Figs. 6(a)–(d), respectively, for various particle diameters. These figures show that if d_p is reduced (in order to obtain a less dispersive profile at the end of pressurization, Fig. 5b), the result is a much larger pressurization time. Also, although the reduction of d_p leads to an approach of the equilibrium situation during blowdown as well, the result is again a much larger blowdown time. The global result in a PSA unit would be a decrease of productivity if the purity and recovery are to be maintained, the reverse also being true (for the same productivity, lower purity and recovery are obtained). On the contrary, the increase of B_p does not suffer from these problems. The comparison between these simulations clearly shows once more that the use of large-pore adsorbents is a good choice for the reduction of intraparticle mass transfer resistances in a PSA process. Figure 7 shows the effect of d_p on pressurization and blowdown times.

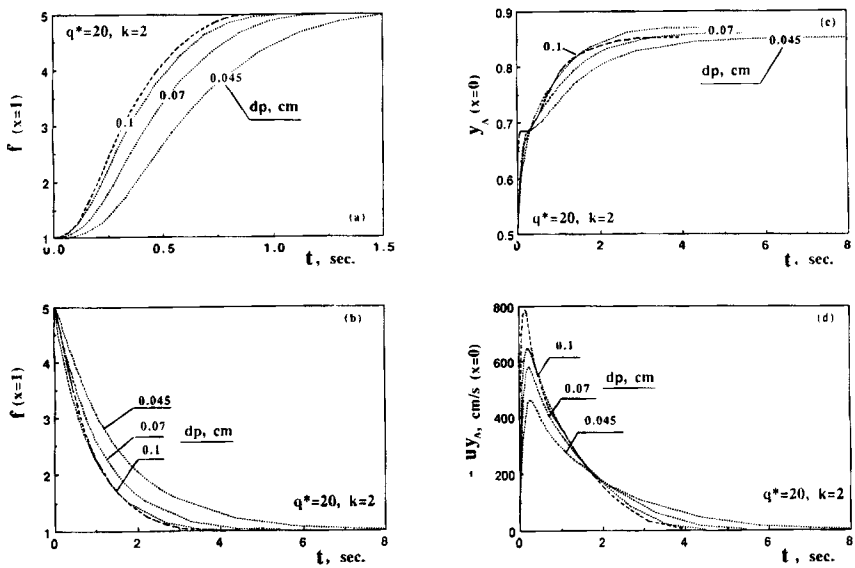

FIG. 6. Effect of particle size d_p (d_p = 0.1, 0.07, and 0.045 cm) on the bed dynamics (k = 2, ··· Case B, ---- Case C). (a) History of reduced total pressure f at the closed end ($x = 1$) during pressurization. (b) History of reduced total pressure f at the closed end ($x = 1$) during blowdown. (c) History of adsorbable species mole fraction y_A at the bed outlet ($x = 0$) during blowdown. (d) History of adsorbable species mole flux ($-uy_A$) at the bed outlet ($x = 0$) during blowdown.

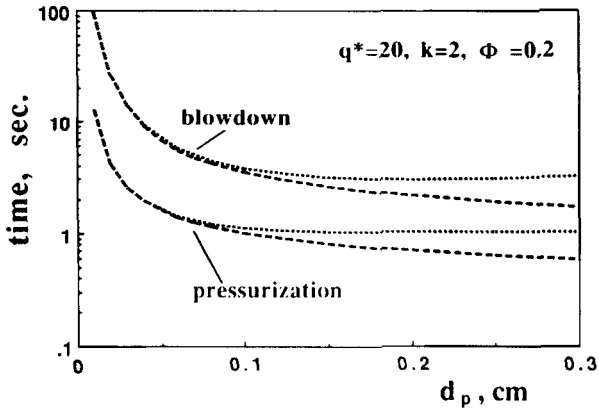

FIG. 7. Pressurization and blowdown times as functions of the particle diameter d_p ($q^* = 20$, $k = 2$, $\Phi = 0.2$, ··· Case B, ---- Case C).

CONCLUSIONS

Pressurization and blowdown of an adsorption bed were studied using three models: equilibrium, diffusion, and diffusion/convection. Simulation results show that the influence of the nature of the adsorption equilibrium isotherm is almost the same for the three models. The penetration distance is lower and the pressurization amount is higher with a Langmuir ($k = 2$) than with a linear ($k = 1$) isotherm; at the end of blowdown, more adsorbable species remain in the bed when a Langmuir isotherm is used. The presence of intraparticle resistances leads to a more dispersive axial mole fraction profile with the diffusion model, the profile approaching the equilibrium situation when intraparticle convection is present. Also, the bed is better regenerated during blowdown when going from the diffusion model to the equilibrium model, showing that intraparticle convection improves both the pressurization and the blowdown steps of a PSA unit.

The enhancement of mass transport due to convection is more clearly seen in blowdown when a nonuniform mole fraction profile initially exists in the bed.

If only the final axial mole fraction profiles are considered, the equilibrium situation can be approached by one of two strategies: either increasing the particle permeability B_p or decreasing the particle diameter d_p. Nevertheless, if a global performance criterion, taking into account productivity, purity, and recovery, is considered, the situation is quite different. In fact, the reduction of d_p leads to a large increase of both the pressurization and the blowdown times, i.e., to a decrease of the productivity for the same

purity and recovery or vice versa, while the increase of B_p has only a marginal effect on those operation step times.

NOTATION

b_4, b_5, b_6	dimensionless constants stated in Table 1
B_p	permeability of the adsorbent (cm^2)
c	total concentration in the bulk fluid phase (mol/cm^3)
c'	total concentration in the fluid inside the adsorbent (mol/cm^3)
c_A	concentration of Species A in the bulk fluid (mol/cm^3)
c_0	total concentration in the bulk fluid at the atmospheric pressure (mol/cm^3)
c_h	total concentration at high pressure P_h (mol/cm^3)
d_p	adsorbent particle diameter (cm)
D_{ax}	axial dispersion coefficient (cm^2/s)
D_e	effective diffusivity (cm^2/s)
$\tilde{D}_e$	"apparent" effective diffusivity (cm^2/s)
D_{mo}	molecular diffusivity at atmospheric pressure (cm^2/s)
D_K	Knudsen diffusivity (cm^2/s)
f	dimensionless total concentration in the bulk fluid phase
f'	dimensionless total concentration in the fluid inside the particle
f_0	dimensionless initial total concentration in the bulk fluid phase
f_0'	dimensionless initial total concentration in the fluid inside the particle
k	constant for the normalized isotherm, Table 1
k_1, k_2	Langmuir isotherm constants
L	bed length (cm)
l	slab thickness (cm)
N	dimensionless total mole flux from the bulk fluid to the adsorbent
N_A	dimensionless mole flux of Species A from the bulk fluid to the adsorbent
P	pressure in the bulk fluid (Pa)
P_0	atmospheric pressure (Pa)
P_h	high pressure (Pa)
P_l	low pressure (Pa)
ΔP_0	pressure drop across the bed under steady-state (Pa)
Pe	Peclet number
P'	pressure in the fluid inside particle (Pa)

q^* constant for the normalized isotherm stated in Table 1
q_A adsorbed phase concentration of Species A (mol/cm^3)
t time (s)
u superficial velocity in the bulk fluid (cm/s)
u_0 superficial velocity at the bed inlet under steady-state (cm/s)
u^* dimensionless velocity in the bulk fluid
v intraparticle velocity (cm/s)
v_0 reference intraparticle velocity (cm/s)
v^* dimensionless intraparticle velocity
x dimensionless axial coordinate in the bed
y_A mole fraction of Species A in the bed
y'_A mole fraction of Species A in the fluid inside the adsorbent
y_0 mole fraction of Species A initially in the bed
z axial coordinate in the bed (cm)
z' space coordinate in the adsorbent (cm)

Greek Letters

α ratio between time constant for intraparticle diffusion and space time, Table 1
$\tilde{\alpha}$ α referred to the "apparent" effective diffusivity
α_0 reference parameter, Table 1
β_I constant defined in Table 1
β_R ratio between the half thickness of the slab and bed length, Table 1
ϵ bed porosity
ϵ_p adsorbent porosity
Φ pressure ratio ($\Phi = P_l/P_h$)
λ intraparticle Peclet number, Table 1
λ_0 intraparticle Peclet number at reference conditions, Table 1
μ fluid viscosity (g/cm·s)
ρ_0 fluid density (g/cm^3)
θ time reduced by the reference space time
τ_f tortuosity factor for the particle
τ_0 reference space time (s)

Acknowledgments

Financial support from FUNDAÇÃO ORIENTE, JNICT, NATO CRG 890600, and EEC JOULE 0052 is gratefully acknowledged.

REFERENCES

1. Hart, J., M. Battrum, and W. J. Thomas, "Axial Pressure Gradients during Pressurization and Depressurization Steps of a PSA Gas Separation Cycle," *Gas Sep. Purif., 4,* 97 (1990).
2. Lu, Z. P., J. M. Loureiro, M. D. LeVan, and A. E. Rodrigues, "Effect of Intraparticle Forced Convection on Gas Desorption from Fixed-Bed Containing 'Large-Pore' Adsorbents," *Ind. Eng. Chem. Res., 31,* 1530 (1992).
3. Lu, Z. P., J. M. Loureiro, A. E. Rodrigues, and M. D. LeVan, "Pressurization of Adsorption Beds. II—Effect of the Momentum and Equilibrium Relations on the Isothermal Operation," *Chem. Eng. Sci.,* In Press.
4. Lu, Z. P., J. M. Loureiro, M. D. LeVan, and A. E. Rodrigues, "Dynamics of Pressurization and Blowdown of an Isothermal Adsorption Bed: Intraparticle Diffusion/Convection and Equilibrium Models," *AIChE J., 38*(6), 857 (1992).
5. Nir, A., and I. Pismen, "Simultaneous Intraparticle Forced Convection, Diffusion and Reaction in a Porous Catalyst I," *Chem. Eng. Sci., 32,* 35 (1977).
6. Rodrigues, A. E., B. Ahn, and A. Zoulalian, "Intraparticle Forced Convection Effect in Catalyst Diffusivity Measurements and Reactor Design," *AIChE J., 28,* 541 (1982).
7. Rodrigues, A. E., Z. P. Lu and J. M. Loureiro, "Residence Time Distribution of Inert and Linearly Adsorbed Species in Fixed-Bed Containing 'Large-Pore' Supports: Applications in Separation Engineering," *Chem. Eng. Sci., 46,* 2765 (1991).
8. Rodrigues, A. E., J. M. Loureiro, and M. D. LeVan, "Simulated Pressurization of Adsorption Beds," *Gas Sep. Purif., 5,* 115 (1991).
9. Rodrigues, A. E., Z. P. Lu, J. M. Loureiro, and M. D. LeVan, *Pressurization of Adsorption Beds,* Paper Presented at the NSF-CNRS Workshop on Adsorption Processes for Gas Separation, Gif-sur-Yvette, France, 1991.
10. Sundaram, N., and P. Wankat, "Pressure Drop Effects in the Pressurization and Blowdown Steps of Pressure Swing Adsorption," *Chem. Eng. Sci., 43,* 123 (1988).
11. Zhong, G. M., F. Meunier, S. Huberson, and J. B. Chalfen, "Pressurization of a Single Component Gas in an Adsorption Column," *Ibid., 47,* 543 (1992).